



HAL
open science

In situ Monitoring of the Oxidation of Coated and Uncoated Austenitic Stainless Steels at Temperatures Lower than 600 °C: Part A Coating Screening

L. Brissonneau, A. Mathieu, F. Navacchia, Henri Buscail, F. Riffard, R. Roland, C. Issartel, S. Perrier

► To cite this version:

L. Brissonneau, A. Mathieu, F. Navacchia, Henri Buscail, F. Riffard, et al.. In situ Monitoring of the Oxidation of Coated and Uncoated Austenitic Stainless Steels at Temperatures Lower than 600 °C: Part A Coating Screening. *Oxidation of Metals*, 2021, 96 (3-4), pp.213-230. 10.1007/s11085-021-10055-6 . hal-03435784

HAL Id: hal-03435784

<https://uca.hal.science/hal-03435784>

Submitted on 16 Dec 2021

HAL is a multi-disciplinary open access archive for the deposit and dissemination of scientific research documents, whether they are published or not. The documents may come from teaching and research institutions in France or abroad, or from public or private research centers.

L'archive ouverte pluridisciplinaire **HAL**, est destinée au dépôt et à la diffusion de documents scientifiques de niveau recherche, publiés ou non, émanant des établissements d'enseignement et de recherche français ou étrangers, des laboratoires publics ou privés.

In-situ monitoring of the oxidation of coated and uncoated austenitic stainless steels at temperatures lower than 600 °C. Part A: Coating screening.

L. Brissonneau ^a, A. Mathieu ^a; F. Navacchia ^a; H. Buscail ^b F. Riffard ^b, R. Roland ^b, C. Issartel ^b, S. Perrier ^b

^a CEA-DES-IRENE-DTN Cadarache F-13108 Saint-Paul-Lez-Durance, France

^b Université Clermont Auvergne, LVEEM, 43000 Le Puy en Velay

laurent.brissonneau@cea.fr ; henri.buscail@uca.fr

Keywords: High Temperature Corrosion, Stainless Steel, Oxygen Sensor, La based coatings, LiNbO₃ reduction...

Abstract

The lithium niobate used in ultrasonic transducer for liquid metal fast nuclear reactors is prone to a reduction leading to a rapid short circuit of the sensor in operating conditions. Oxygen consumption on stainless steel sensor's walls was suspected to be the cause of the reduction. Impedance spectroscopy monitoring around 600 °C under different O₂ partial pressure shows that the reduction limit is above the equilibrium pressure of iron oxides. As the housing material (304L) cannot be easily changed, various coating solutions enhancing the passivation of the steels were investigated. Sol-gel Lanthanum coatings show the best behavior when tested by TGA at 800 °C. However, *in situ* monitoring of the oxygen consumption by an oxygen sensor close to operating condition, shows that it was not enough protective.

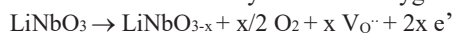
Introduction

Liquid metals are very interesting coolants for nuclear fast reactors but one of their main drawbacks, is their opacity. Sensors have to be developed in order to locate assemblies, detect gas formation and detect failures in the structure (1). CEA Cadarache develops a high temperature (> 550 °C) ultrasonic transducer for liquid metal fast nuclear reactors (Sodium or Lead Fast Reactors or Lead Bismuth Eutectic Accelerator Driven System for example [1]). Former similar sensors were prone to rapid short circuit in operation when the piezo-electric element (LiNbO₃) was not used in open air. These failures were associated with the reduction of the piezo-electric crystal. As working with a sensor in open air in a liquid metal reactor generates hard constraints (air must be constantly pumped from the reactor building into the sensor, through the roof and the rotating plugs), solutions were investigated to fix the crystal reduction. Oxygen consumption on stainless steel sensor's walls was suspected to be the cause of the reduction. This has been proven by impedance monitoring under different partial pressure as described in the first part of the paper. As the housing material (304L) cannot be easily changed (compatibility in liquid metal environment, sensor fabrication process...), coating solutions enhancing the passivation of the steels were first investigated. During a three years collaboration between LVEEM and CEA Cadarache, several protective methods were investigated to limit the rate of O₂ consumption, aiming to limit the formation of Fe₂O₃ and to decrease the kinetic of diffusion of iron through the chromia layer, which eventually leads to hematite formation. The evaluation of these solutions is presented in the second part of the paper. The test of the most promising one in more representative conditions is reported in the final part.

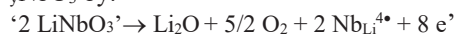
Deoxidation of lithium niobate

It is well known that heating lithium niobate (LN) at 300-1100 °C under vacuum [2] or Ar/H₂ [3] leads to the formation of such defects which induces a coloration of the crystal. Smyth found that the conductivity vary as P(O₂)^{-1/4} in reducing conditions [4]. Ohlendorf et al. found an increase of the conductivity above 10⁻¹⁵ atm at 750 °C under H₂/H₂O atm osphere [5].

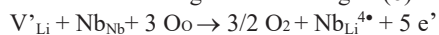
The reduction of the crystal at low oxygen partial pressure can be represented by the following equations:



Leading to the formation of F center defects, or more likely for congruent lithium niobate, which is deficient in Li, Li_{1-y}NbO₃ by:



Which is less energetics according to (6). Or considering substoichiometric LN enables the loss of a unit cell:



as the formation of additional Nb⁴⁺, which are traditional defects in Li depleted LiNbO₃, are more stable than oxygen vacancies. This interpretation is supported by density measurements [4] and optical absorption [6]. This implies that the increase of the conduction is rather by polarons in the antisites (Nb_{Li}^{3•}) than by oxygen vacancies [6] and that part

of the LN is transformed into Li_2O at reduction (loss of crystal units). Here, the number of new defects $\text{Nb}_{\text{Li}}^{4*}$ formed by reduction would be small towards their initial concentration in the congruently LN [4]...

According to Garcia Caebes et al. [2], if the crystal is close to stoichiometry, these new defects are localized close to the surface. This would mean that the surface of the crystal would transform into Li_2O , leaving the Nb ions in the Li vacancies. Sugak [3] noticed a different behavior after several oxidation/reduction cycles and attributed it to irreversible changes in the near surface regions. However, Ohlendorf does not detect large loss of Li at 750 °C by Mass Spectrometry [5].

In-situ impedance measurements were performed on LiNbO_3 (or LN) to determine the critical oxygen partial pressure at which it starts to lose its high impedance properties. Three z-axis oriented monocrystalline LiNbO_3 pellets (thickness 0.82 mm, congruent LN, deficient in Li) were tested simultaneously at CEA Cadarache in the AMPHORE facility (Assemblage et Mesures à Pressions d'Hydrogène et d'Oxygène RéguléEs), built by LEPMI (CRNS/Université Grenoble), at constant temperature (600 °C) and different oxygen partial pressures controlled by a GENAIR® (SETNAG) apparatus. Their impedance was monitored using impedance spectrometry using a Solartron 1260A (0.1V, 10^7 to 1 Hz). Oxygen partial pressures down to 10^{-19} atm were obtained using Ar, when Ar/H₂ 3% was needed for lower pressures. Tests were performed at constant temperature (600 °C) and different oxygen partial pressures 10^{-4} to 10^{-23} atm. Oxygen partial pressure can be monitored upstream or downstream the pellets. In general, several hours are needed before the equilibrium pressure is reached in the system.

In the first tests at high oxygen partial pressures (between 10^{-4} and 10^{-8} atm) only one well defined semi-circle is observed on the Nyquist plot, even after a 3 days test (Figure 1a). The corresponding resistance is close to the one that can be calculated from the relationship between conductivity and temperature by Jorgensen et al. [7]. It vanishes at low $P(\text{O}_2)$ (10^{-23} atm, only an inductive contribution is observed, from the set up), which means that the crystal is reduced. After re-oxidation in air at 600 °C, a second semi-circle is observed at intermediate frequencies for oxygen pressures higher than 10^{-19} atm (Figure 1b). Around $P(\text{O}_2) = 10^{-18}$ atm for 4 days, a tenfold decrease of the total impedance was observed, the second circle disappeared.

After 4 hours oxidation in air at 615 °C, pellets are tested at $P(\text{O}_2) = 10^{-11}$ and 10^{-19} atm. The impedance of the second circle increased. Decreasing pressure to $P(\text{O}_2) = 10^{-23}$ atm, the impedance of the pellets becomes negligible since the first measurements.

After re-oxidation in air, the impedance of the pellets under air is now five times higher than in the very first tests, the second semi-circle impedance becomes comparable to the first one. Setting pressure to $P(\text{O}_2) = 10^{-21}$ atm, the impedance decreases with fast kinetics (faster than one hour) at $P(\text{O}_2) = 10^{-21}$ atm (Figure 1c). The second semi-circle disappeared first, when the first semi-circle is divided by 2 in the first 15 minutes, and by more than four in the 15 following minutes. All the three pellets exhibits the same behavior. After the test, the pellets turn from transparency to grey.

The evolution of the SI diagrams can be interpreted as follows: at the first measurements, only the semi-circle corresponding to crystal impedance is observed. After reduction and re-oxidation of the crystal, the appearance of the second semi-circle at intermediate frequencies is a blocking contribution of the grain boundaries. Therefore, one can assume that a phase transformation occurs when reduction is strong enough and that during re-oxidation, the new crystals do not necessarily grow epitaxially with the former z-axis orientation (however, X Ray diffraction performed on the pellets after the tests did not reveal any changes: only the (001) plan diffraction remains visible on the diffractogram). This texture would also lead to the increase of the grain impedance, as the impedance might not be strictly isotropic. At each reduction/re-oxidation cycle, the number of grains increases and then the contribution of the grain boundaries too.

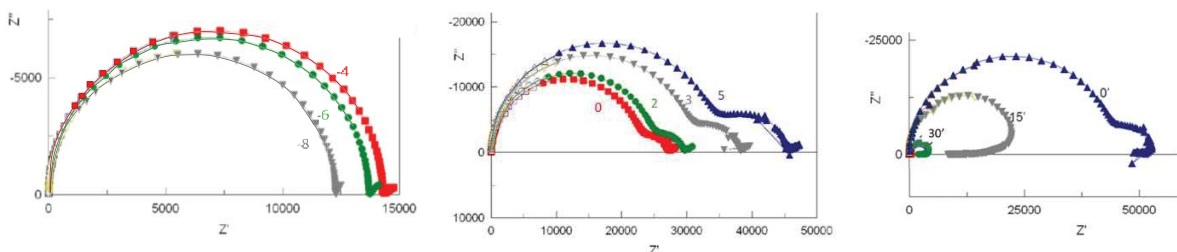


Fig. 1 Nyquist plot of a LiNbO_3 pellet tested at 600 °C a) first measurements, at $P(\text{O}_2) = 10^{-4}$ to 10^{-8} atm (numbers = logP) ; b) at $P(\text{O}_2) = 10^{-11}$ atm, increasing time (in hours) after two reduction and oxidation cycles ; c) at $P(\text{O}_2) = 10^{-21}$ atm and 600 °C at different times (numbers in minutes).

Halvarsson et al. [8] show that the oxides formed by oxidation in O₂ and H₂O on 304L at 600 °C are corundum-type Cr rich α - (Fe,Cr)₂O₃ –base oxide- and Fe rich (Fe,Cr,Mn)₂O₃ (islands, when water is added to O₂). These two oxides have equilibrium oxygen partial pressures (<10⁻²⁴ atm) lower than the one needed for high and quick crystal reduction as observed in our experiments (10⁻²¹ atm at 600 °C). As a consequence, the oxidation of the metal in the sensor must be slowed so that the oxygen partial pressure does not decrease at values lower than 10⁻²⁰ atm.

TGA analysis of La coated and uncoated steels

Depending of sensor's geometry, a total conversion of the air embedded in the sensor would lead to a Fe₂O₃ layer thickness between 0.1 μ m and 0.2 μ m on the 304L walls. This is only twice the thickness of the base oxide obtained in one week at 600 °C on uncoated 304L (9). As the sensors are expected to work several years at 550 °C, the formation of the Fe rich (Cr,Fe)₂O₃ layer has to be prevented. Based on LVEEM's proposals, several protective methods were investigated to limit the rate of O₂ consumption by oxidation. The common idea was to limit the formation of Fe₂O₃ by favoring the formation of the Cr₂O₃ chromia layer limiting the diffusion process. The three methods tested were respectively based on: pre-oxidation under dry low O₂ atmosphere, protection by SiO₂ deposits [4] and protection by a lanthanum coating [5], which are described later. These protective methods were tested at LVEEM at 800 °C, in air, during 70 h, on 304L coupons 25*15*1 mm³, SiC 320 polished and weighed by thermogravimetric analysis (TGA). The results are compared in Fig 2.

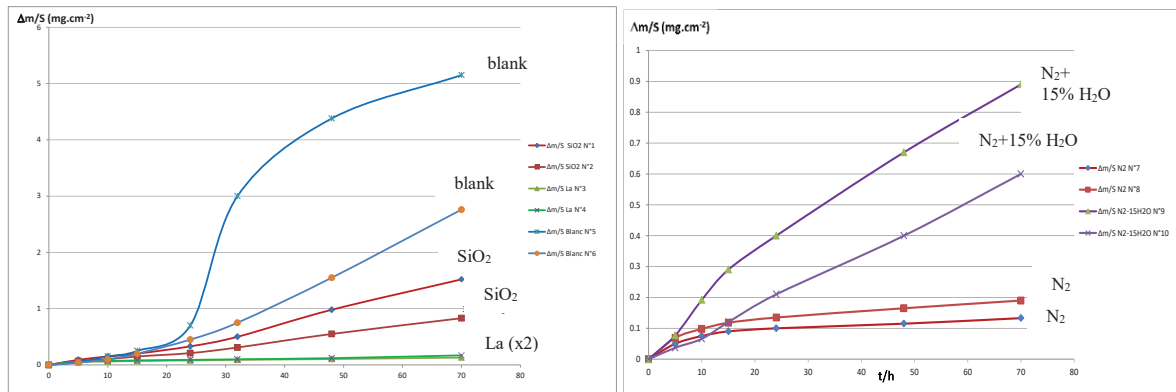


Fig 2: Mass changes of the 304L steel specimens during oxidation, in air at 800 °C, 70 h. Comparison of various protection treatments : a) blank coupons (blue), PSZ SiO₂ coated (red) and La coated (green) ; b) comparison of blank 304L oxidation in N₂ and N₂ containing 15 vol. % water vapor.

304L coupons tested without any protection exhibited high and scattered oxidation rates (blue curve in Fig. 2a). The first protection method consists in heating the steels under dry nitrogen flow containing 15 ppm O₂ at 800 °C, during 70 h. The oxidation rate is low (Fig.2b). Back scattered electrons images and SEM evidenced that the well adherent thin layer consists in Mn_{1.5}Cr_{1.5}O₄ and Cr₂O₃.

As expected from literature data [8-9] oxidizing 304L under an atmosphere containing water (15 vol. %) is much more detrimental than under dry atmosphere (Fig. 2b). The kinetic of oxide formation is faster and the phase detected contained iron: (Fe_{0.6}Cr_{0.4})₂O₃, nodules of Fe₃O₃ and manganese chromite Mn_{1.5}Cr_{1.5}O₄ (ICDD 33-0892) with iron in substitution. H₂O can absorb preferentially on the surface [11] and form Si and Cr volatile compounds [8] which leads to a chromium depletion of the metal close to the surface and then favors the presence of iron in the oxide layer. Moreover, water can lead to the formation of a porous oxide and to the formation of protons in the oxide layer. The presence of protons might increase the concentration of cationic vacancies and hence increase the oxidation rate. Protons may also play an oxidizing role at the metal interface [11].

PSZ SiO₂ coating (1 μ m thick) is obtained by dipping the steel in a polysilazane solution. It presents some cracks. At 800 °C under air for 70 hours, the kinetic of oxidation is linear and at least twice lower than without protection (Fig. 2a). Mn_{1.5}Cr_{1.5}O₄, Fe_{0.7}Cr_{1.3}O₃ and SiO₂ are detected by XRD (see Figure 4a) and SEM. On most of the surface, the homogeneous very thin and adherent layer is Mn_{1.5}Cr_{1.5}O₄ (according to EDS mapping and XRD analysis) the metal under the surface is chromium depleted; remnants of SiO₂ deposit can be observed. Less discrepancy between these

two samples is observed than between the blank specimens. This discrepancy is attributed to surface preparation and iron containing oxide nodules nucleation, which becomes less predominant when a coating is applied, as more uniform oxide layers are formed. Unfortunately, the deposit is not completely protective; some big oxide nodules ($\approx 50 \mu\text{m}$) can be observed, which grow internally and externally. The internal part is rich in $(\text{Cr},\text{Ni},\text{Fe})_2\text{O}_3$, whereas the external part is composed of Fe rich $(\text{Cr},\text{Fe})_2\text{O}_3$.

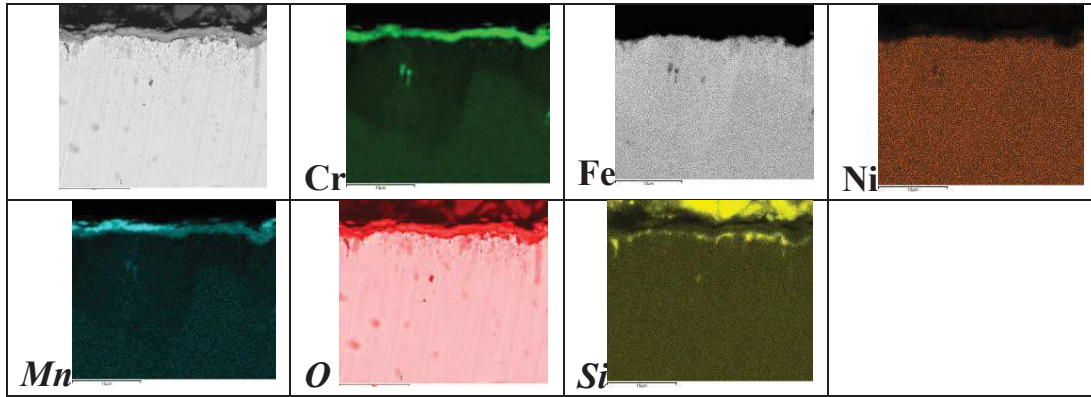


Fig. 3: SEM and elemental EDS mapping of the layer grown on 304L after 70 h under N_2 -15 ppm O_2 .

The best results were obtained by applying a $0.5 \mu\text{m}$ thick lanthanum sol gel coating. It consists in a sol gel deposition of a solution containing $\text{La}(\text{NO}_3)_3$ then fired 72 h at $800 \text{ }^\circ\text{C}$ in order to form stable oxides on the surface. The La-coating decreases the oxidation rate by one order of magnitude (Figure 2a), with less scattering between samples. The mass gain is parabolic, and La formed likely a LaCrO_3 phase, according to XRD (Figure 4b). La, Mn and Cr are also observed by SEM/EDS (Figure 5) in the thin oxide layer. The scale structure is due to the La-doping of the chromia layer, which favors anionic diffusion (rather than cationic iron diffusion) a low growth rate and good adherence [12]. XRD also shows that the formation of Cristobalite on La-coated specimens. This oxide might also play a protective role. This was already observed on a cerium deposit on a silicon containing alloy [13]. $\text{Mn}_{1.5}\text{Cr}_{1.5}\text{O}_4$ was also detected by XRD.

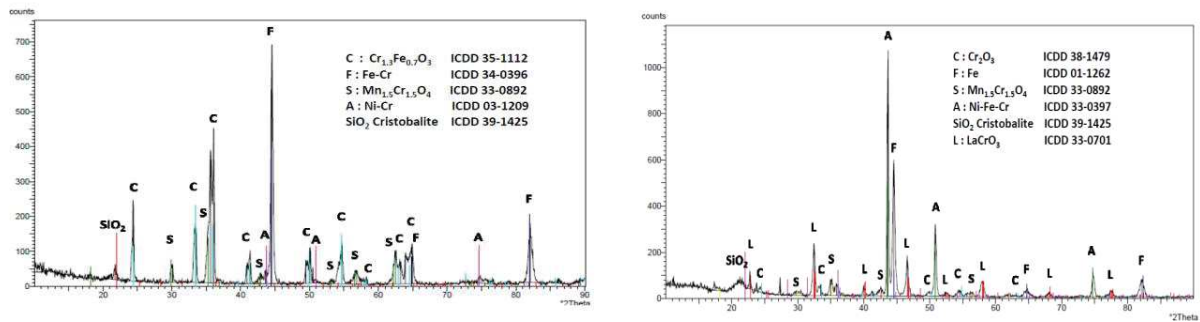


Fig. 4: a) XRD pattern of 304L + SiO_2 PSZ ; b) XRD pattern on La coated specimens. After oxidation in air, 70 h at $800 \text{ }^\circ\text{C}$. ICDD: International Center of Diffraction Data.

As the La coted specimens exhibit the best results, cross TGA tests were performed in both laboratories (on SETARAM's Setsys evolution 1750 and TG-DTA 92-1600) on 304L coupons ($\approx 11*8*1 \text{ mm}^3$ or $25*15*1 \text{ mm}^3$, SiC 320 polished) coated by the operator of each laboratory. They are compared with similar blank samples. The tests were performed at $800 \text{ }^\circ\text{C}$, in air, during 72 h on non-fired samples (the water vapor is supposed to be about 50% Relative Humidity then about 1 vol.% Absolute Humidity). These conditions were chosen to be able to detect the very small weight gains even if these are far from reactor's operating conditions ($550 \text{ }^\circ\text{C}$) and to detect the effect of any art skill of the operator in the deposition. As the coated steels must be fired in similar conditions ($800 \text{ }^\circ\text{C}$, 72 h) to form the protective layer, the expected behavior under oxidation in real conditions is the one observed at the end of the test (provided the samples behaves in similar ways at $550 \text{ }^\circ\text{C}$ and $800 \text{ }^\circ\text{C}$).

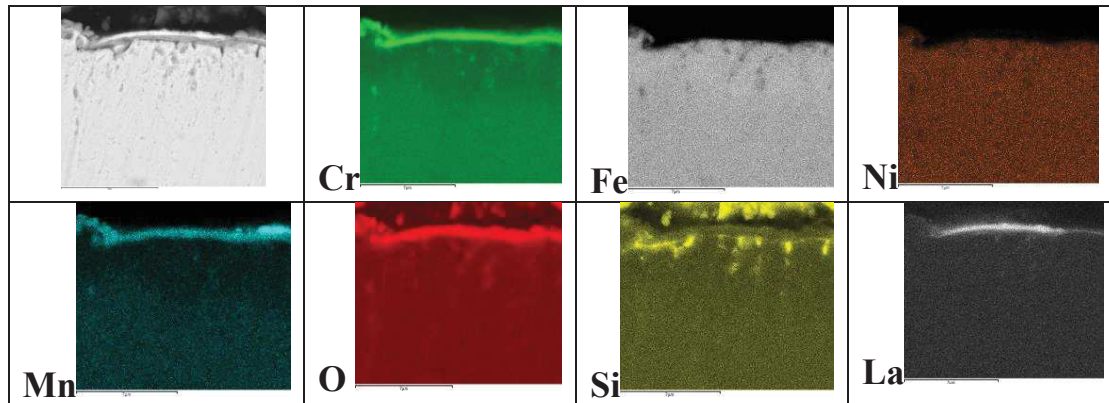


Fig. 5: SEM and elemental EDS mapping of La coated 304L after oxidation in air 800 °C, 70 h.

A comparison of the TGA analyses in the two labs is reported in Figure 6. Results are very close (provided that the 8 first hours are removed for CEA's tests, as performed in Figure 6left), whatever the operator or the TGA apparatus. The final mass gain is about 0.1 mg.cm⁻² for all coated coupons. For uncoated steel, the final gain mass is higher than 0.3 mg.cm⁻². XRD analyses evidenced the formation of hematite Fe₂O₃ and chromia Cr₂O₃ on uncoated steels; sometimes the layers are spalled from the samples. On coated steels, a spinel, likely (Mn,Fe)(Mn,Fe,Cr)₂O₄, Cr₂O₃, LaCrO₃ and chromium rich (Fe,Cr)₂O₃ were observed (as in Figure 4b), which are assumed to be rather protective. The results are confirmed by SEM cross section observations. The mass variation q can be fitted with a parabolic law with time, $q=k.t^{1/2}$, where $k = 0.0124 \text{ mg.cm}^{-2}.\text{h}^{-1}$ for the coated steels. If such a law also stands at 550 °C, the reaction rate must be divided by 3000 by decreasing the temperature from 800 °C to 550 °C to obtain a total consumption of the O₂ in the sensor in less than one year. It entails that the activation energy of constant k must be higher than 250 kJ.mol⁻¹. The activation energy for the diffusion of O²⁻ or Cr³⁺ in Cr₂O₃ for example are quite scattered but all above 250 kJ.mol⁻¹, though the calculated migration energy itself is smaller (lower than 100 kJ.mol⁻¹) [14].

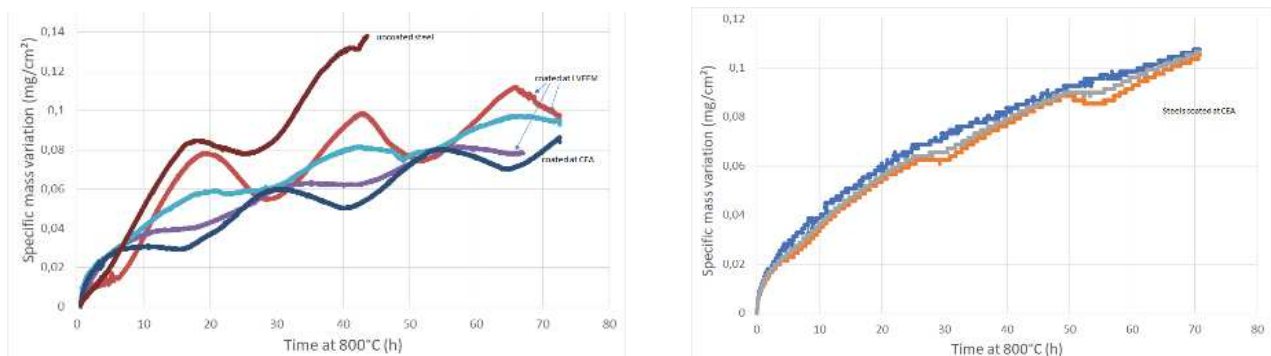


Fig. 6: TGA analyses at CEA (left) and at LVEEM (right) of coated and uncoated (brown, at left) 304L specimens in air at 800 °C.

In situ monitoring in representative conditions

To check the efficiency of the coatings at low temperature (< 600 °C), tests were performed in a device allowing the monitoring of oxygen *in situ*. 304L steels cylinders (ϕ 20 mm h 29 mm) extracted from a plain tube (provided by Lugand Cr 18.0% Ni 8.1% Mn 1.5% Si 0.45% Fe bal.) were La coated, fired (800 °C, 72 h, in air) and welded to a pre-oxidized (1200 °C, 6 h, in air) Fecralloy tube provided by Goodfellow in which a zirconia oxygen sensor (ZOS, Micropoas® from SETNAG) is inserted. A TGA test shows that the mass change for heat treated Fecralloy is negligible at 800 °C, in air. Thus, any oxygen consumption in the system can be attributed to the La coated steel. The nuts and the line (for ZOS connection) are out of the furnace, after cooling fans, so their temperature is so low (< 80 °C) that

they do not contribute to oxygen consumption. The ZOS and the vent/feed line are connected with VCR nuts, which ensure that no oxygen leak will disturb the oxidation monitoring. The tightness of the device is tested before each test. The ZOS allows to monitor the oxygen consumption at very low rates. This system is very similar to the real one, where oxygen pressure is not constant. Then it can be checked in representative conditions (low temperatures, no oxygen feeding, constant volume), if the oxygen consumption by the coated steel is slow enough to not reach critical oxygen pressure values (LiNbO₃ reduction, < 10⁻²⁰ atm) before the expected lifetime of a sensor (at least one year). The initial atmosphere in the sample could be air, argon or partial or complete vacuum (from primary pump). Campaign of tests were performed at ≈530 °C, ≈550 °C and 580 °C at different original P(O₂). The lower temperature limit of the ZOS is about 520 °C. As no P(O₂) variation could be observed under this limit, the gas was often inserted in the device when the target temperature had been reached. The temperature inside the cylinder was given by the thermocouple of the ZOS (and is reported in the following figures simultaneously with P(O₂)). Four different systems were tested: at first, two empty La coated 304L cylinders; after testing, these two cylinders were cut, grinded with SiC paper, one was La coated and fired, the other not, both were filled with a LN pellet and welded to the Fecralloy tube for new campaigns of tests. Tests procedure, their interpretation and the modelling will be detailed in a coming paper [15]. We present here only the most relevant features.

Low P(O₂) tests (< 10⁻⁵ atm)

When tests were performed under argon or vacuum, the first readings of the P(O₂) were already very low: under 10⁻¹⁷ atm. It decreased rapidly until 10⁻²³ atm, then much slowly (the pressure could stabilize after a few hours). An example without LN pellet is reported in Figure 8a. The stationary values were obtained at about 10⁻²⁶ atm at 525 °C, 10⁻²⁵ atm at 550 °C and 10⁻²⁴ atm at 570 °C. When the LN pellet had been added in the device, the pressure decrease appeared slower around 10⁻²² atm. This is consistent with the LN oxygen release attributed to impedance decrease at pressure lower than 10⁻²⁰ atm observed by impedance spectroscopy (see above). The final pressure was close to the one calculated with HSC 5.1 for Fe₂O₃ between 550 °C (2.7x10⁻²⁶ atm) and 600 °C (2.5x10⁻²⁴ atm).

When tests started with a higher P(O₂) and could be performed on a long duration (2 days), the P(O₂) consumption from intermediate pressures (>10⁻⁵ atm) and equilibrium pressure (<10⁻²⁴ atm) could be observed, as in Figure 8b. The pressure decrease was exponential between 10⁻⁷ to 10⁻¹³ atm. Then a strong decrease of the oxidation rate was observed between 5.10⁻¹³ and 10⁻¹⁴-10⁻¹⁶ atm; a 2 °C step increase in the device was observed at ≈5.10⁻¹³ atm. Then, the oxygen consumption rate increased again (but slower than at high pressure) and finally slowed down at about 10⁻²¹ atm (even if in one case, no LN pellet was present). It is reported that a buffering effect involving CO₂ and CO can be observed at P(O₂) around 10⁻¹³ -10⁻¹⁶ atm [16], which might explain the oxidation rate decrease.

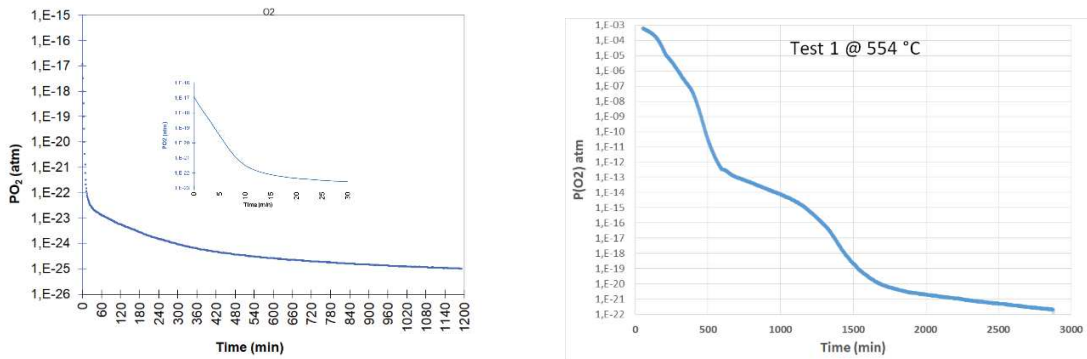


Fig. 7 : test at low pressure a) test 3 under vacuum at 556 °C (insert first half hour) ; b) test 1, in argon at 554 °C

P(O₂) tests in intermediate pressure ranges (10⁻¹ – 10⁻⁴ atm)

An example of oxygen monitoring during a test between 4x10⁻² and 3x10⁻² atm at 525 °C is shown in Figure 8 (right). In most cases, a linear interpolation can be proposed. On the period investigated for one test at these intermediate pressures (about 3 days), only a limited pressure range could be investigated. The kinetic constants increase with the temperature. However, it was also observed that the constants tend to decrease when the pressure range decreases. Even, at the lower pressure tested (6 to 1x10⁻⁴ atm), data are better fitted by a 2nd order polynomial expression as: P(O₂) = P^o(O₂) - k₁t + k₂t² (k₁ and k₂ >0).

The linear constant varies from $1.2 \times 10^{-6} \text{ atm} \cdot \text{min}^{-1}$ (at $1.5 \times 10^{-3} \text{ atm}$, $537 \text{ }^\circ\text{C}$) to $6.3 \times 10^{-6} \text{ atm} \cdot \text{min}^{-1}$ (at 10^{-2} atm , $579 \text{ }^\circ\text{C}$). During the campaign with one system, the observed variations are consistent: increase of the constants with pressure and temperature. However, the kinetics appears to be faster for system 1 than for systems 2 and 3. In these two last cases, the La coatings were applied by the same person, and experience was gained from the first application in system 1. Then, it is believed that the quality of the deposit has an influence on the steel resistance against oxidation and then on the kinetic constant.

The system 4 was not La coated. The first test of the campaign began at $558 \text{ }^\circ\text{C}$. The oxygen consumption was very fast and can be described by a logarithmic law $P(\text{O}_2) = P^\circ(\text{O}_2) - k \cdot \log(t)$. After reaching the equilibrium value, a test was performed in air, and then at intermediate pressure. The linear kinetic constant in that test is twice lower than for systems 2 and 3 at a similar temperature.

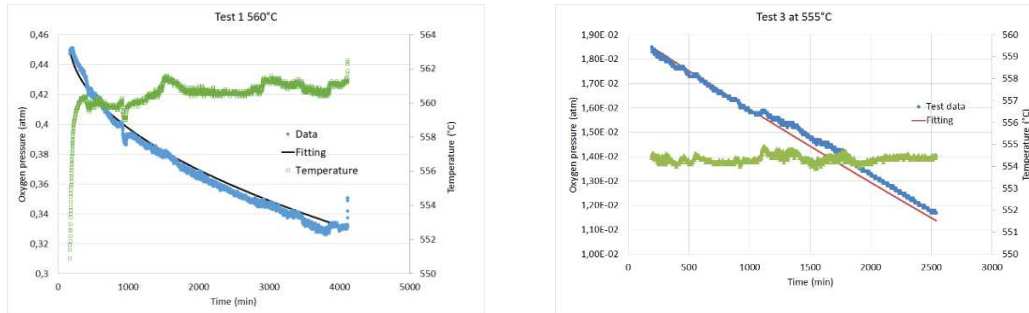


Fig. 8 In situ oxygen pressure monitoring of a La-coated steel at $555 \text{ }^\circ\text{C}$, at high initial pressure (left) and at intermediate initial pressure (right)

$P(\text{O}_2)$ tests at high pressure ranges ($> 10^{-1} \text{ atm}$)

Only a few tests were performed at high pressure, at $T \approx 555 \text{ }^\circ\text{C}$, as the decrease rate is rather low. The data are well fitted on the range 0.44-0.32 bars by a quadratic law $P(\text{O}_2) = P^\circ(\text{O}_2) - k_1 t^{1/2}$ ($k_1 > 0$), as shown in Fig. 9 left. For the system 4 (uncoated steel), the test at high pressure was performed just after the initial, fast and total oxygen consumption.

Discussion of the $P(\text{O}_2)$ monitoring tests.

It will be derived in a next paper [15] that the pressure variation in the system can be approximately described by the following equation,

$$P = P_0 + y_0/G \left(1 - \sqrt{1 + \frac{2k(t - t_0)}{y_0^2}} \right)$$

Where P_0 and y_0 are the O_2 pressure and initial oxide thickness at time t_0 , G relates the increase of the oxide layer thickness to the pressure variation in the system.

And provided that the kinetic is limited only by the cationic diffusion (and assuming an exponent $1/n = 8$ for a +III cation (16)), $k = (z + 1)D_v \Delta V_n^{eq}$, $k = k_{p,T} \cdot P(\text{O}_2)^{1/n}$; the assumption of cationic diffusion limitation will be discussed in the paper to come ([15]).

where z is the charge of the cation, D_v the diffusion coefficient of its vacancy and ΔV^{eq} the vacancy gradient at equilibrium between the internal and external sides of the oxide.

The equation can be approximated by a linear decrease at low pressure [15], as observed in the experiments. It was found, for each experiment at a defined temperature, a unique constant k whatever was the pressure range, but the initial thickness y_0 input in the calculation is one order of magnitude lower than expected from the mass gain after the heat treatment of the La-deposit. For the lower pressure ranges, a more complex model must be used to fit the data.

From the kinetic constant k found by the fitting, the pressure decrease in the sensor due to wall oxidation can be modelled. From the first results, it was found that the La coating only delays the total consumption from a few days to some months. This is not a long enough operation time in reactor.

Conclusion

Impedance spectroscopy measurements confirms that the reduction of the LiNbO_3 , that induces the failure of high temperature US transducers, can occur at $600 \text{ }^\circ\text{C}$ for pressures obtained at equilibrium between a stainless steel and its

oxide. Several protective ways were tried to limit the kinetic of oxygen consumption: oxidation at low pressures, SiO₂ coatings from PSZ and La coatings based on lanthanum nitrate. The latter exhibits the best behavior, and it was found from TGA measurements at 800 °C that promising behavior could be expected at lower temperature.

The La sol-gel coating on steel was then tested *in situ* with a ZOS at temperature around 550 °C. The measurements were performed on limited pressure ranges due to the low kinetic. At low pressures, the kinetic of oxygen consumption is linear and rather parabolic at high pressures. Some fittings have been obtained from a simple model and extrapolation was performed for the real situation. Although it behaves much better than uncoated steels (total air consumption in a few hours), the *in situ* monitoring of O₂ partial pressure evidenced that this solution appears to be unable to fix the reduction of LiNbO₃ in reactor operating conditions: total oxygen consumption is expected in a few months. It is believed that the authors that the deposits in the in-situ tests were rather similar to the one obtained after TGA experiments. It is also believed that the presence of cracks would not allow enough surface of steel to be in contact with air to dramatically enhance the oxygen consumptions. So defects in the deposits are not thought as the cause of their failure, which seems rather intrinsic. New solutions will be tested, based on different approaches, as the limitation of the oxidation kinetics appears to be a too hard challenge in this application.

Acknowledgements: The CEA Cadarache thanks Mr Ch. Duriez from IRSN Cadarache for performing the TGA.

References

1. Navacchia, F.; Brissonneau, L.; Lhuillier, C. Procédé de fabrication d'un capteur piézoélectrique et capteur piézoélectrique obtenu par un tel procédé. Patent CEA, 2018, 70874 FR1854631, WO 2019 228862/A1.
2. García-Cabaes, A.; Sanz-García, J. A.; Cabrera, J. M.; Agulló-López, F.; Zaldo, C.; Pareja, R.; Polgár, K.; Raksányi, K.; Fölvári, I., *Physical Review B* **1988**, *37* (11), 6085-6091.
3. Sugak, D.; Zhydachevskii, Y.; Sugak, Y.; Buryy, O.; Ubizskii, S.; Solskii, I.; Schrader, M.; Becker, K. D., *J. Phys.-Condes. Matter* **2007**, *19* (8).
4. Smyth, D. M., *Ferroelectrics* **1983**, *50* (1-4), 419-428.
5. Ohlendorf, G.; Richter, D.; Sauerwald, J.; Fritze, H. In *High-Temperature Electrical Conductivity and Electromechanical Properties of Stoichiometric Lithium Niobate* Bunsen Colloquium: Diffusion and Reactions in Advanced Materials September 27th – 28th, 2007, , Clausthal-Zellerfeld, Germany, Diffusion Fundamentals: Clausthal-Zellerfeld, Germany, 2008; pp 6.1-6.7.
6. Schirmer, O. F.; Imlau, M.; Merschjann, C.; Schoke, B., *J. Phys.-Condes. Matter* **2009**, *21* (12), 29.
7. Jorgensen, P. J.; Bartlett, R. W., *J. Phys. Chem. Solids* **1969**, *30* (12), 2639-&.
8. Halvarsson, M.; Tang, J. E.; Asteman, H.; Svensson, J. E.; Johansson, L. G., *Corrosion Science* **2006**, *48* (8), 2014-2035.
9. Asteman, H.; Svensson, J. E.; Norell, M.; Johansson, L.-G., *Oxidation of Metals* **2000**, *54* (1-2), 11-26.
10. Jacob, Y. P.; Haanappel, V. A. C.; Stroosnijder, M. F.; Buscail, H.; Fielitz, P.; Borchardt, G., *Corrosion Science* **2002**, *44* (9), 2027-2039.
11. Issartel, C.; Buscail, H.; Wang, Y.; Rolland, R.; Vilasi, M.; Aranda, L., *Oxidation of Metals* **2011**, *76* (3-4), 127-147.
12. (a) Buscail, H.; Issartel, C.; Riffard, F.; Rolland, R.; Perrier, S.; Fleurentin, A., *Oxidation of Metals* **2014**, *81* (1-2), 127-138; (b) Buscail, H.; Issartel, C.; Riffard, F.; Rolland, R.; Perrier, S.; Fleurentin, A.; Josse, C., *Appl. Surf. Sci.* **2011**, *258* (2), 678-686; (c) Golightly, F. A.; Wood, G. C.; Stott, F. H., *Oxidation of Metals* **1980**, *14* (3), 217-234; (d) Hou, P. Y.; Stringer, J., *J. Phys. IV* **1993**, *3* (C9), 231-240; (e) Issartel, C.; Buscail, H.; Rolland, R.; Perrier, S.; Fleurentin, A., *Oxidation of Metals* **2013**, *80* (5-6), 467-478; (f) Karimi, N.; Buscail, H.; Riffard, F.; Rabaste, F.; Cuff, R.; Issartel, C.; Caudron, E.; Perrier, S., Effect of Lanthanum Sol-Gel Coating on the Oxidation Behaviour of the AISI 304 Steel at 1000 degrees C. In *High Temperature Corrosion and Protection of Materials 7, Pts 1 and 2*, Steinmetz, P.; Wright, I. G.; Galerie, A.; Monceau, D.; Mathieu, S., Eds. Trans Tech Publications Ltd: Stafa-Zurich, 2008; Vol. 595-598, pp 733-741; (g) Pint, B. A., *Oxidation of Metals* **1996**, *45* (1-2), 1-37; (h) Riffard, F.; Fondard, J.; Moulin, P.; Perrier, S.; Buscail, H., *Oxidation of Metals* **2014**, *81* (1-2), 191-201.
13. Buscail, H.; Sotto, P.; Larpin, J. P., *J. Phys. IV* **1993**, *3* (C9), 309-315.
14. Vaari, J., *Solid State Ionics* **2015**, *270*, 10-17.
15. Brissonneau, L.; Mathieu, A.; Navacchia, F., **to come**.
16. Sarrazin, P.; Galerie, A.; Fouletier, J., *Les mécanismes de la corrosion sèche. Une approche cinétique*. EDP Sciences: Les Ulis, 2000.